Modeling of phase diagrams for bcc magnetic alloys

D. A. Contreras-Solorio, F. Mejía-Lira, and J. L. Morán-López
Instituto de Fisica, Universidad Autónoma de San Luis Potosí, 78000 San Luis Potosí, San Luis Potosí, Mexico

J. M. Sanchez
Henry Krumb School of Mines, Columbia University, New York, New York 10027
(Received 18 December 1987)

The phase diagram of a model bcc binary alloy with one magnetic component is studied using the tetrahedron approximation of the cluster variation method. The model includes first- and second-nearest-neighbor chemical and magnetic interactions between atoms of spin $\frac{1}{2}$. The ground-state structures at zero magnetic field and their ranges of stability with regard to the interaction parameters are obtained using the method of linear inequalities introduced by Kanamori and by Allen and Cahn. Temperature-composition phase diagrams are calculated for ordering alloys with antiferromagnetic interactions.

I. INTRODUCTION

Several theoretical and experimental studies have shown that the interplay between magnetism and chemical order has pronounced effects on the equilibrium and metastable phase diagrams of binary transition metal alloys.[1] For example, it is well documented that spatial long-range order in the Ni-Pt system reduces appreciably the Curie temperature relative to that of the disordered alloys.[2] A similar effect has been reported in the Fe-Al system.[3] Conversely, magnetism has a strong effect on the alloy spatial order. For example, it is generally agreed that the order-disorder transition observed at low temperatures in Co_3Pt is a consequence of the magnetic interactions[3]. Another example is the Fe-Co system where it has been shown that the order-disorder transition is intimately linked to magnetism[4] and, in particular, that the asymmetry with concentration in the order-disorder transition temperature is dictated by the asymmetry in the Curie temperature.[5]

In recent years, bcc alloys with one magnetic component have attracted considerable theoretical interest.[3,6] These studies were largely motivated by the complex behavior observed in the Fe_xAl_{1-x} (Refs. 7 and 8) and in the Fe_xSi_{1-x} (Refs. 9 and 10) systems which, at low temperatures, adopt either the DO_3 or the $B2$ structure depending on the concentration of the transition-metal component.

Owing to the complexities involved in the first-principles treatment of alloy phase equilibrium, particularly for the magnetic transition metals, theoretical studies are generally based on simple phenomenological models. Despite the intrinsic limitations of these phenomenological models, they have been very valuable in the study of general trends of magnetic and nonmagnetic systems. For example, many features related to the interplay between magnetism and spatial order can be satisfactorily modeled by considering only short-range interactions between nearest-neighbor (NN) and next-nearest-neighbor (NNN) atoms.[1-6] These simple models have been investigated extensively at finite temperatures using the Bragg-Williams approximation. Recently, higher-order approximations as well as Monte Carlo simulations have been used to study magnetic alloys with both the bcc[11] and the fcc[2,12] structures.

Here we present a systematic study of the ground-state structures and of the equilibrium properties at finite temperatures for a model bcc binary alloy with one spin-$\frac{1}{2}$ magnetic component. Both NN and NNN chemical and magnetic pair interactions are included in the model. In the absence of an external magnetic field, we find 12 different ground-state configurations. The ranges of stability of the 12 ground-state configurations are obtained using a method of linear inequalities similar to that introduced originally by Kanamori[13] and by Allen and Cahn,[14] and more recently by Sanchez and de Fontaine.[15] The method of linear inequalities has been used by several authors to investigate the ground states of nonmagnetic fcc (Refs. 13–15) and bcc (Ref. 16) binary alloys with pair interactions up to fifth neighbors. In Sec. II we briefly present the method used to determine the ground states and discuss the results obtained for the magnetic bcc alloys.

The temperature-composition phase diagrams for prototype magnetic alloys are calculated by means of the cluster variation method[17] (CVM) using, as the basic cluster, the irregular tetrahedron formed by NN and NNN pairs. The results of the finite-temperature calculations together with a brief outline of the CVM is given in Sec. III. Concluding remarks are presented in Sec. IV.

II. GROUND STATES

Most of the ordered superstructures reported experimentally in magnetic bcc alloys can be obtained as ground states of an Ising model Hamiltonian with only NN and NNN pair interactions, the latter being essential in order to stabilize the commonly observed DO_3 structure. Thus, in the present model, we assume that the energy of the

system is given by

$$E = -\tfrac{1}{2}\sum_{n=1}^{2} V_n N_{AB}^{(n)} - \sum_{n=1}^{2} J_n (N_{A\uparrow A\uparrow}^{(n)} + N_{A\downarrow A\downarrow}^{(n)} - 2N_{A\uparrow A\downarrow}^{(n)}) , \quad (1)$$

where V_n and J_n are, respectively, the chemical and magnetic interactions between nth neighbors ($n=1,2$), and where $N_{ij}^{(n)}$ is the number of nth-neighbor pairs of species i and j. In Eq. (1), A is the magnetic component and $A\uparrow$ $A\downarrow$ represent the two allowed spin configurations. The effective chemical interactions V_n are defined in terms of the atomic interaction $V_{ij}^{(n)}$ between atomic species i and j by

$$V_n = V_{AA}^{(n)} + V_{BB}^{(n)} - 2V_{AB}^{(n)} . \quad (2)$$

Positive magnetic interactions J_n favor aligned magnetic moments between nth neighbors, whereas a positive value of the chemical interaction V_n favors nth-neighbor pairs of unlike chemical species.

The problem of characterizing the ground states consists of minimizing the energy E, which is linear in the configurational variables $N_{ij}^{(n)}$, for all possible values of the interaction parameters V_n and J_n. For a given cluster approximation, in our case the irregular tetrahedron, it can be shown that all possible states of order of the system are located inside a convex polyhedron in configurational space. The configurational polyhedron is defined by the condition that all cluster probabilities must be positive and properly normalized to unity. The dimension of configuration space is determined by the number of independent probabilities corresponding to the maximum cluster or, alternatively, by the number of all possible cluster correlation functions.[18] Since the configurational polyhedron is convex, the energy for any state of order may be written as[15]

$$E = \sum_{k=1}^{K} \rho_k E_k , \quad (3)$$

where K is the total number of vertices of the polyhedron, E_k is the energy corresponding to vertex k, and ρ_k are non-negative barycentric coordinates obeying the relation

$$\sum_{k=1}^{K} \rho_k = 1 . \quad (4)$$

In addition to Eq. (4), the barycentric coordinates ρ_k generally obey a linear constraint arising from the fixed concentration of the alloy. As seen from Eqs. (3) and (4), the vertices of the configurational polyhedron correspond to all possible ground-state superstructures.

The range of stability with respect to the interaction parameters V_n and J_n is given by an hypercone with extreme rays defined by the normals to all faces of the configurational polyhedron converging to the vertex in question.[15] The hypercone forms the so-called dual of the configurational polyhedron. Finally, ground-state phase diagrams may be constructed by means of lower dimensional sections of the dual polyhedron in interaction space.

The analysis of the binary alloy with one magnetic component in the tetrahedron approximation gives 13 vertices of the configurational polyhedron. The tetrahedron configurations for all 13 ordered structures ($Z_m, m=1,\ldots,13$) are depicted in Fig. 1. We find that the vertex corresponding to the ferrimagnetic structure Z_2 is not stable for zero magnetic field, which reduces the total number of possible ground states to 12. The structures corresponding to the 12 ground states can be described in terms of the four interpenetrating sublattices shown in Fig. 2. For pure component A, there are three ground

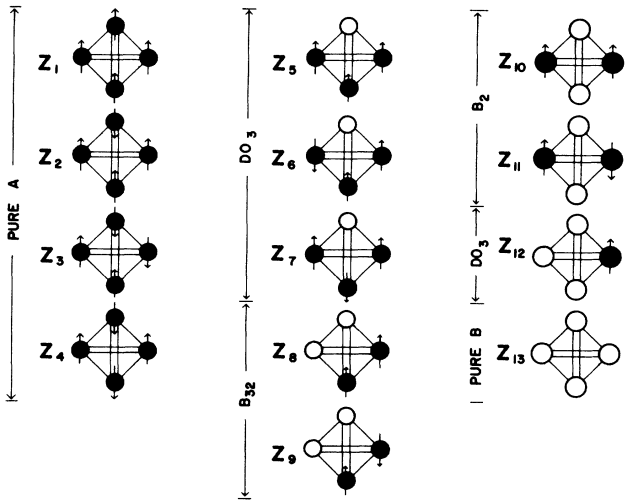

FIG. 1. The tetrahedron configurations for all possible ground states of the bcc alloy with one magnetic component.

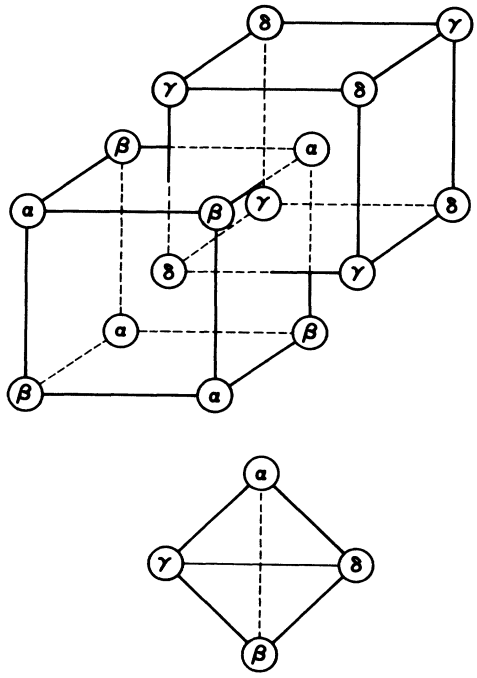

FIG. 2. The four interpenetrating sublattices in the bcc structure. Also shown is the irregular tetrahedron straddling sublattices, α, β, γ, and δ.

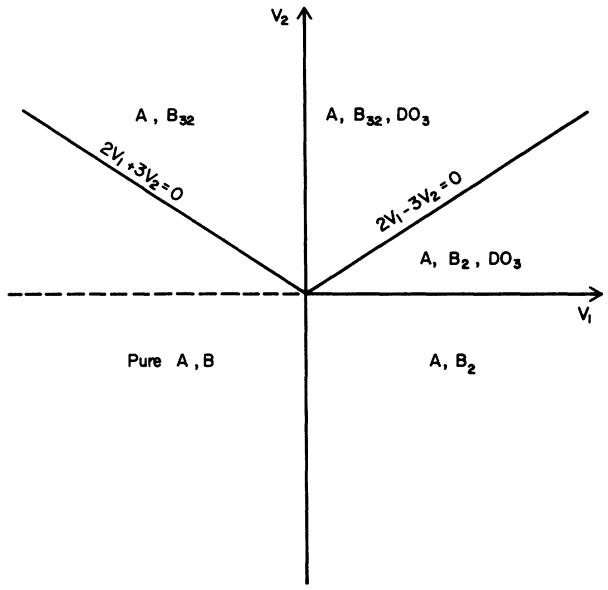

FIG. 3. Ground-state phase diagram for bcc nonmagnetic binary alloy with NN (V_1) and NNN (V_2) chemical interactions (Ref. 14).

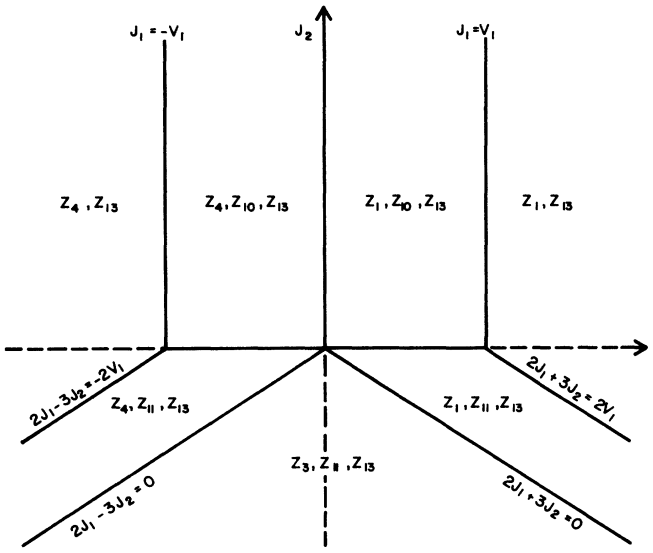

FIG. 5. Ground-state phase diagram in the NN (J_1) and NNN (J_2) magnetic interactions space for a bcc binary alloy with one magnetic component and chemical interactions given by $V_1 > 0$ and $V_2 < 0$.

states corresponding to the ferromagnetic phase (Z_1) and to two antiferromagnetic states with the same symmetries as the $B32$ (Z_3) and $B2$ (Z_4) ordered alloys. For stoichiometry A_3B, there are also three ground states corresponding to ferromagnetic ordering (Z_5) and to antiferromagnetic ordering (Z_6 and Z_7) on the magnetic sublattices. At stoichiometry AB there are ferro- and antiferromagnetic phases with chemical ordering that corresponds, in the paramagnetic state, to the $B32$ (Z_8 and Z_9) and $B2$ (Z_{10} and Z_{11}) structures. Finally, for alloys rich in the nonmagnetic component B the ground state is the DO_3 structure (Z_{12}) and, for pure B, the disordered $A2$ structure (Z_{13}).

In Fig. 3, we include the ground-state phase diagram obtained by Allen and Cahn[14] for nonmagnetic bcc alloys with chemical NN and NNN pair interactions V_1 and V_2,

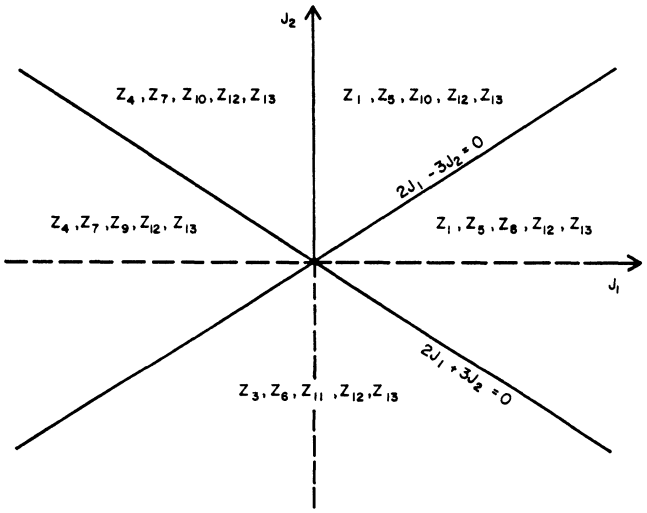

FIG. 4. Ground-state phase diagram in the NN (J_1) and NNN (J_2) magnetic interactions space for a bcc binary alloy with one magnetic component and chemical interactions $V_1 = V_2 = 0$.

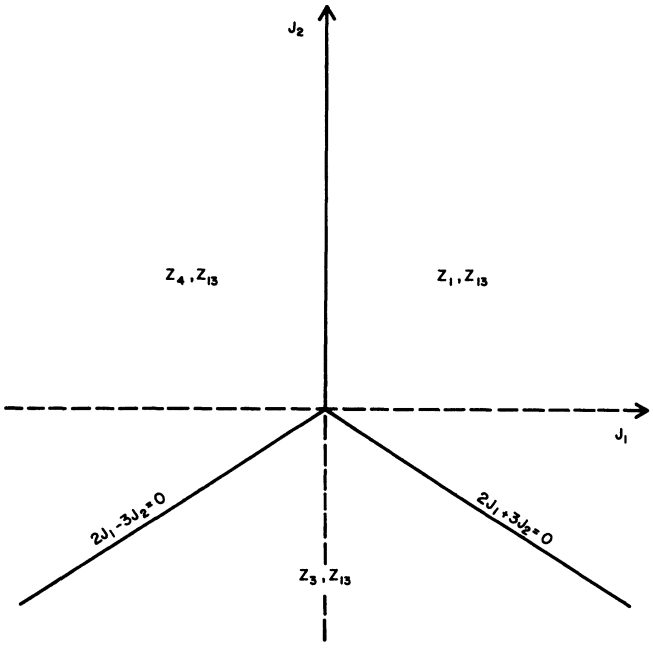

FIG. 6. Ground-state phase diagram in the NN (J_1) and NNN (J_2) magnetic interactions space for a bcc binary alloy with one magnetic component and chemical interactions given by $V_1 < 0$ and $2V_1 + 3V_2 < 0$.

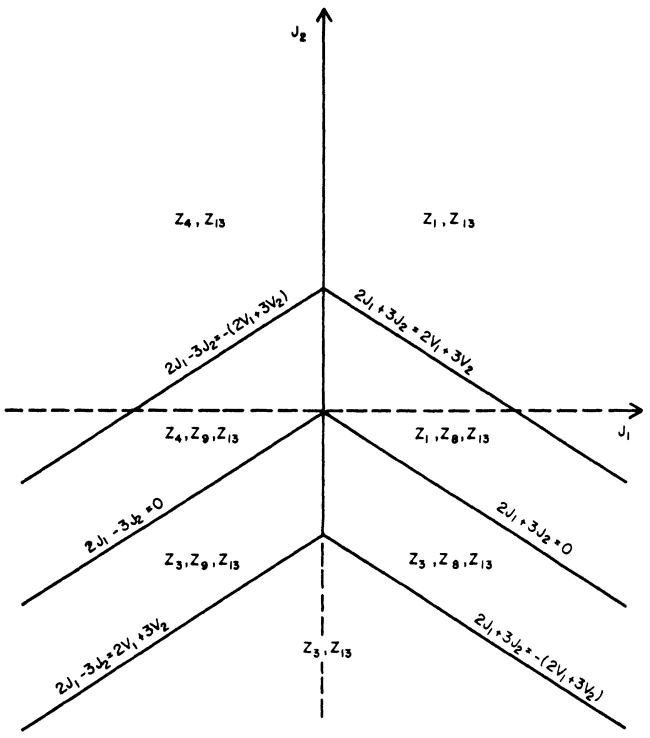

FIG. 7. Ground-state phase diagram in the NN (J_1) and NNN (J_2) magnetic interactions space for a bcc binary alloy with one magnetic component and chemical interactions given by $V_1 < 0$ and $2V_1 + 3V_2 > 0$.

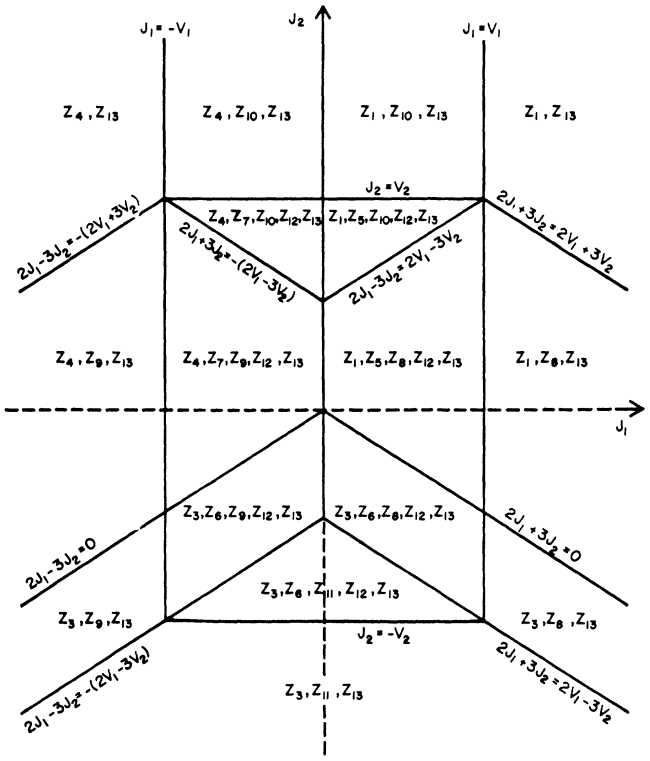

FIG. 8. Ground-state phase diagram in the NN (J_1) and NNN (J_2) magnetic interactions space for a bcc binary alloy with one magnetic component and chemical interactions given by $V_1 > 0$ and $2V_1 - 3V_2 < 0$.

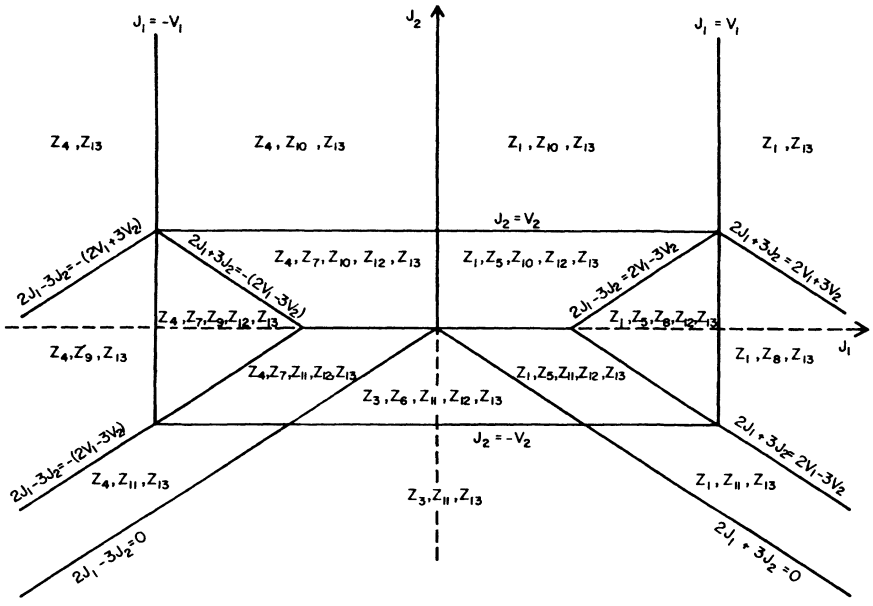

FIG. 9. Ground-state phase diagram in the NN (J_1) and NNN (J_2) magnetic interactions space for a bcc binary alloy with one magnetic component and chemical interactions given by $V_2 > 0$ and $2V_1 - 3V_2 > 0$.

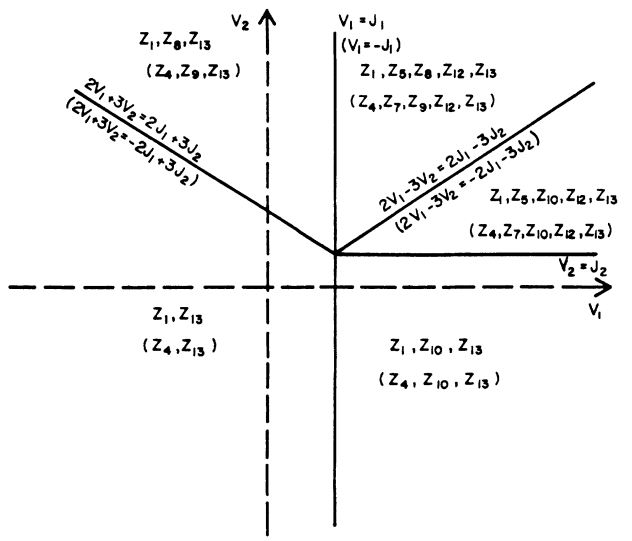

FIG. 10. Ground-state phase diagram in the NN (V_1) and NNN (V_2) chemical interactions space for a bcc binary alloy with one magnetic component and magnetic interactions given by $J_1 > 0$ and $J_2 > 0$. The ground-state structures shown in parentheses are for magnetic interactions obeying $J_1 < 0$ and $J_2 > 0$.

respectively. A similar phase diagram for a system with only magnetic interactions (for zero magnetic field) is shown in Fig. 4. As can be seen in Fig. 3, there are five distinct regions for different values of V_1 and V_2: (i) $V_1 > 0$, $V_2 < 0$; (ii) $V_1 < 0$, $2V_1 + 3V_2 < 0$; (iii) $V_1 < 0$, $2V_1 + 3V_2 > 0$; (iv) $V_1 > 0$, $2V_1 - 3V_2 < 0$; and (v) $V_2 > 0$, $2V_1 - 3V_2 > 0$. The ground-state phase diagrams

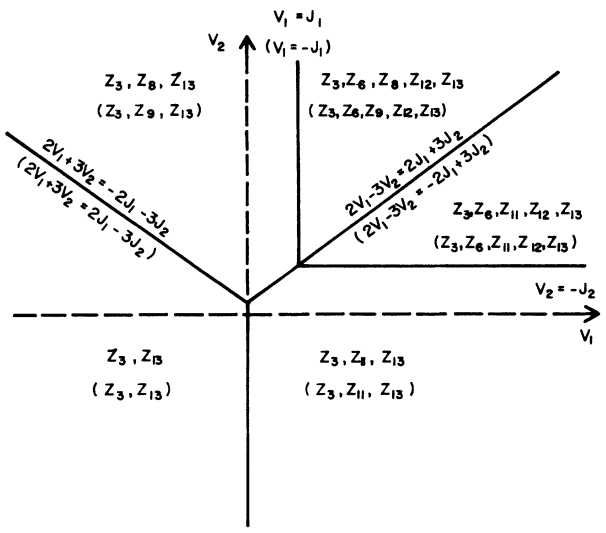

FIG. 11. Ground-state phase diagram in the NN (V_1) and NNN (V_2) chemical interactions space for a bcc binary alloy with one magnetic component and magnetic interactions given by $J_1 > 0$ and $2J_1 + 3J_2 < 0$. The ground-state structures shown in parentheses are for magnetics interactions obeying $J_1 < 0$ and $2J_1 - 3J_3 > 0$.

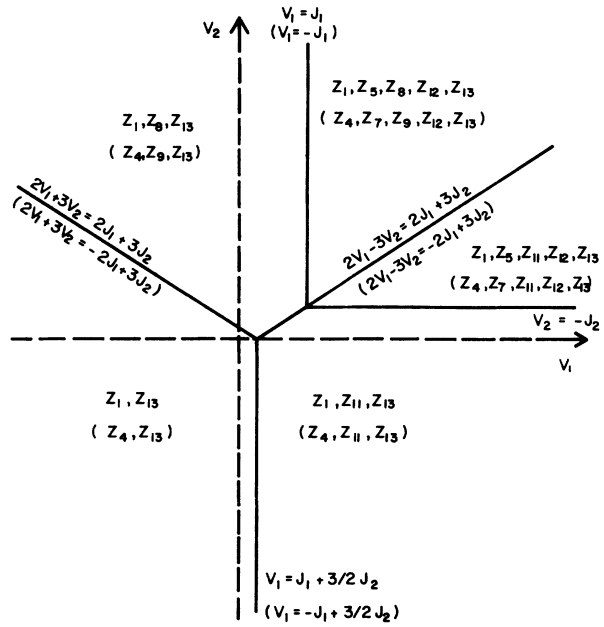

FIG. 12. Ground-state phase diagram in the NN (V_1) and NNN (V_2) chemical interactions space for a bcc binary alloy with one magnetic component and magnetic interactions given by $J_2 < 0$ and $2J_1 + 3J_2 > 0$. The ground-state structures shown in parentheses are for magnetics interactions obeying $J_2 < 0$ and $2J_1 - 3J_2 < 0$.

corresponding to regions (i) to (v) are, respectively, shown in Figs. 5 to 9. These diagrams depict the range of magnetic interactions, J_1 and J_2, for which a set of ordered phases Z_m (see Fig. 1) are the ground states for alloys with compositions ranging from pure A to B. The ground-state phase diagrams in terms of the chemical interactions V_1 and V_2 are shown in Fig. 10 for $J_1 > 0$, $J_2 > 0$ ($J_1 < 0$, $J_2 > 0$); in Fig. 11 for $J_1 > 0$, $2J_1 + 3J_2 < 0$ ($J_1 < 0$, $2J_1 - 3J_2 > 0$); and in Fig. 12 for $J_2 < 0$, $2J_1 + 3J_2 > 0$ ($J_2 < 0$, $2J_1 - 3J_2 > 0$).

III. FINITE-TEMPERATURE CALCULATIONS

In this section we describe the calculations of the temperature-composition phase diagrams for prototype magnetic alloys with positive NN chemical interactions ($V_1 > 0$), and NNN chemical interactions $V_2 = 0.5V_1$. We investigate two cases characterized by antiferromagnetic exchanges J_1 (NN) and J_2 (NNN) given by (i) $J_1 = -0.125V_1$, $J_2 = -0.1V_1$ and (ii) $J_1 = -0.125V_1$, $J_2 = -0.05V_1$. The set of interactions used in both cases correspond to the ground-state diagram shown in Fig. 9: For case (i), the ground states are Z_3, Z_6, Z_{11}, Z_{12}, and Z_{13} whereas for case (ii) the set of ground states are given by the structures Z_4, Z_7, Z_{12}, and Z_{13}.

The free energy of the magnetic alloy as a function of temperature and composition is calculated using the tetrahedron approximation of Kikuchi's CVM. The basic configurational variables in this approximation are the probabilities z_{ijkl} of finding an irregular tetrahedron, con-

necting sublattices α, β, γ, and δ shown in Fig. 2, respectively occupied by atomic species i, j, k, and l. In the present case of a binary alloy with one magnetic component, the indices i, j, k, and l can take three values corresponding to atoms $A\uparrow$, $A\downarrow$, and B. The relevant subcluster probabilities, obtained trivially from the z_{ijkl}, are the single-site probability (x_i^{ν}), the NN ($y_{ij}^{\nu\nu'}$) and NNN ($u_{ij}^{\nu\nu'}$) pair probabilities, and the triangle probability $t_{ijk}^{\nu\nu'\nu''}$, where i, j, and k refer to atomic species and where ν, ν', and ν'' refer to the four sublattices α, β, γ, and δ.

The configurational entropy for a general ordered state is given by

$$S=-Nk\left[6\sum_{ijkl}L(z_{ijkl})-3\sum_{ijk}[L(t_{ijk}^{\alpha\gamma\beta})+L(t_{ijk}^{\alpha\delta\beta})+L(t_{ijk}^{\gamma\alpha\delta})+L(t_{ijk}^{\gamma\beta\delta})]\right.$$
$$\left.+\tfrac{3}{2}\sum_{ij}[L(u_{ij}^{\alpha\beta}+L(u_{ij}^{\gamma\delta})]+\sum_{ij}[L(y_{ij}^{\alpha\gamma})+L(y_{ij}^{\alpha\delta})+L(y_{ij}^{\beta\gamma})+L(y_{ij}^{\beta\delta})]-\tfrac{1}{4}\sum_{i}[L(x_i^{\alpha})+L(x_i^{\beta})+L(x_i^{\gamma})+L(x_i^{\delta})]\right] \tag{5}$$

with k Boltzmann's constant, N the total number of points in the lattice, and where $L(x)=x\ln(x)$.

The number of pairs $N_{ij}^{(n)}$ required to compute the configurational energy [see Eq. (1)] are given by

$$N_{ij}^{(1)}=N(y_{ij}^{\alpha\gamma}+y_{ij}^{\alpha\delta}+y_{ij}^{\beta\gamma}+y_{ij}^{\beta\delta})\,, \tag{6a}$$

$$N_{ij}^{(2)}=\tfrac{1}{2}N(u_{ij}^{\alpha\beta}+u_{ij}^{\gamma\delta})\,. \tag{6b}$$

The free energy for a general ordered structure as a function of the variational tetrahedron probabilities z_{ijkl} follows directly from Eqs. (1), (5), (6a), and (6b), and from the fact that the subcluster probabilities appearing explicitly in the free energy are given by partial traces, or sums, of the tetrahedron variables. The final minimization step, required to calculate the equilibrium free energy and probability distribution z_{ijkl} is usually carried out at constant chemical potential and magnetic field; the latter will be taken equal to zero in all our calculations. Different minimization algorithms as well as convenient procedures to construct the phase diagram have been discussed extensively in the literature. In order to solve the minimization equations we have used a successive iterations scheme introduced by Kikuchi.[17] Critical lines in the equilibrium phase diagram were obtained by determining the vanishing of the smallest eigenvalue of the 80×80 matrix of second derivatives of the free energy. The dimension of the second derivatives matrix is given by the number of linearly independent tetrahedron variables $z_{ijkl}(3^4-1)$. First-order transition lines in the temperature-chemical potential space were obtained from the equality of the grand potentials for different phases. In general, these transitions occur between phases of either the same or different symmetry but having different concentrations.

In the tetrahedron approximation used here, all minima of the configurational free energy can be fully characterized using four sublattice magnetizations (m_ν), the average concentration of the nonmagnetic component (x_B), and three chemical long-range order parameters (η_n) defined, respectively, by

$$m_\nu=x_{A\uparrow}^{\nu}-x_{A\downarrow}^{\nu}\quad(\nu=\alpha,\beta,\gamma,\delta)\,, \tag{7a}$$

$$x_B=(x_B^{\alpha}+x_B^{\beta}+x_B^{\gamma}+x_B^{\delta})/4\,, \tag{7b}$$

$$\eta_1=(x_B^{\alpha}+x_B^{\beta}-x_B^{\gamma}-x_B^{\delta})/2\,, \tag{7c}$$

$$\eta_2=(x_B^{\alpha}+x_B^{\gamma}-x_B^{\beta}-x_B^{\delta})/2\,, \tag{7d}$$

$$\eta_3=(x_B^{\alpha}+x_B^{\delta}-x_B^{\beta}-x_B^{\gamma})/2\,. \tag{7e}$$

In the paramagnetic state ($m_\nu=0$, for $\nu=\alpha$, β, and δ), the different types of chemical ordering are given by (i) $\eta_1=\eta_2=\eta_3=0$ for $A2$ structure; (ii) $\eta_1\neq0$, $\eta_2=\eta_3=0$ for the $B2$ structure; (iii) $\eta_2\neq0$, $\eta_1=\eta_3=0$ for $B32$ structure; and (iv) $\eta_1\neq0$, $\eta_2=\eta_3\neq0$ for the DO_3 structure. In what follows we will use the notation $A2$, $B2$, $B32$, and DO_3 to indicate chemical order corresponding to cases (i), (ii), (iii), and (iv) above, irrespective of the magnetic ordering. We note that, in general, the magnetic ordered phases will have lower symmetry than suggested by our simplified notation. The magnetic order itself will be characterized by indicating the sublattices magnetization m_ν.

The calculated phase diagrams—using $V_1>0$, $V_2=0.5V_1$, and $J_1=-0.125V_1$—are shown in Fig. 13 for the case of $J_2/J_1=0.8$ and in Fig. 14 for the case of $J_2/J_1=0.4$. We see from Figs. 13 and 14 that the transition between the paramagnetic phases $A2$(PM) to $B2$(PM) is of second order for all temperatures and concentrations, whereas the $A2$(PM) to DO_3(PM) ordering transition occurring at low temperatures is of first order. We see that for both cases shown in Figs. 13 and 14, the transition from $B2$(PM) to DO_3(PM) is of first order over a small temperature and composition range becoming second order, at a tricritical point, towards the center of the phase diagram. Another feature common to the phase diagrams of Figs. 13 and 14 is the temperature at which

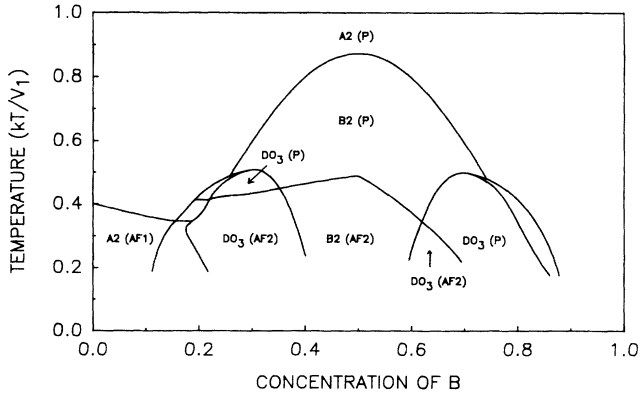

FIG. 13. Temperature-composition phase diagram for a bcc alloy with one magnetic component, calculated using the tetrahedron approximation of the cluster variation method. The pair interactions are $V_1>0$, $V_2=0.5V_1$, $J_1=-0.125V_1$, and $J_2/J_1=0.8$.

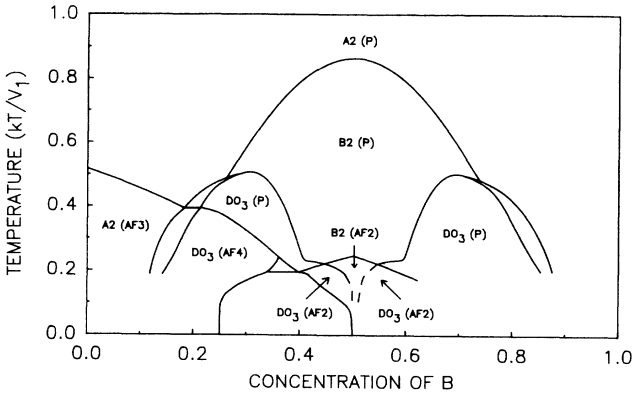

FIG. 14. Temperature-composition phase diagram for a bcc alloy with one magnetic component, calculated using the tetrahedron approximation of the cluster variation method. The pair interactions are $V_1>0$, $V_2=0.5V_1$, $J_1=-0.125V_1$, and $J_2/J_1=0.4$.

the magnetic transition takes place in the stoichiometric $B2$ phase ($x_B=0.5$): in both cases, the transition temperature correlates closely to that of a simple cubic lattice with magnetic interactions given by J_2.

The equilibrium antiferromagnetic phases for the case $J_2/J_1=0.8$, shown in Fig. 13, are $A2$(AF1) with $m_\alpha=m_\delta=-m_\beta=-m_\gamma\neq 0$; DO_3(AF2) with $m_\alpha=m_\beta=0$ and $m_\gamma=-m_\delta\neq 0$; and $B2$(AF2) with $m_\alpha=m_\beta=0$ and $m_\gamma=-m_\delta\neq 0$. We note that all transitions between antiferromagnetic phases are of second order. This is also the case for transitions between para- and antiferromagnetic phases, except for the $A2$(PM) and $A2$(AF1) to DO_3(AF2) transitions which entail simultaneous changes in chemical and magnetic ordering.

A different set of antiferromagnetic phases is seen in Fig. 14 for the case of $J_2/J_1=0.4$: $A2$(AF3) with $m_\alpha=m_\beta=-m_\gamma=-m_\delta\neq 0$; DO_3(AF4) with $m_\alpha=0$, $m_\beta<0$, and $m_\gamma=m_\delta>0$; DO_3(AF2) with $m_\alpha=m_\beta=0$ and $m_\gamma=-m_\delta\neq 0$; and $B2$(AF2) with $m_\alpha=m_\beta=0$ and $m_\gamma=-m_\delta\neq 0$. Unlike the case of Fig. 13, we see that the chemically ordered DO_3 phase now exists with two different antiferromagnetic structures, referred to above and in Fig. 14 as AF2 and AF4. The DO_3(AF4) phase is one of the ground states listed in Fig. 1 (Z_7) and, for concentrations of the nonmagnetic component B near 0.25, it is favored by the configurational energy. For higher concentrations of B, the equilibrium phase is DO_3(AF2) which mediates the transition from the DO_3(AF4) structure to the $B2$(AF2) ground state (Z_{11}). Since the magnetic structures of the DO_3(AF2) and $B2$(AF2) are the same, the transition can be of second order as indicated in Fig. 14. We note, however, that the portion of these transitions which are shown by broken lines in Fig. 14 are uncertain due to numerical difficulties encountered in the computation of eigenvalues in this temperature and composition range.

IV. CONCLUSIONS

The stability of ordered superstructures for bcc binary alloys with one magnetic component was investigated for a simple pairwise model with NN and NNN chemical and magnetic interactions. The energy minimization at $T=0$ K was carried out using the method of linear inequalities from which all ordered ground states were obtained: for zero magnetic field, the analysis reveals 12 possible ground states displaying chemical, ferro- and antiferromagnetic ordering. Despite the simplicity of the interaction Hamiltonian, we find that the most commonly observed ordered structures in real magnetic alloys are represented among the ground states of the model. Furthermore, depending on the sign and relative strength of the chemical and magnetic pair energies, a large number of distinct sets of ground states are possible.

The equilibrium states, free energies, and relative stability at finite temperatures were investigated using the tetrahedron approximation of the CVM. We studied two alloys that, in the paramagnetic state, order in the $B2$(PM) and DO_3(PM) structures. The antiferromagnetic interactions J_1 and J_2 were chosen so as to stabilize the same (Fig. 13) and different (Fig. 14) magnetic structures in the chemically ordered phases. For the case, $J_2/J_1=0.4$ (Fig. 14), the chemically ordered phase of the DO_3 type exists with two different antiferromagnetic structures: DO_3(AF2) and DO_3(AF4) having zero and finite total magnetizations, respectively. General symmetry considerations show that a phase transition between these two phases must be of first order, as shown in the low temperature region of Fig. 14, and therefore these phases can coexist over a range of average concentrations x_B.

ACKNOWLEDGMENTS

This work was partially funded by the National Science Foundation under Grants No. DMR-85-10594 and No. INT-84-09776 and by the Direccion General de Investigación Científica and Superación Académia de la Secretaria de Educación Pública (Mexico) under Grants No. C-86-01-0284 and No. C-86-01-0294. One of us (D.A.C.S.) wishes to acknowledge support from the Consejo del Sistema Nacional de Educación Tecnológica de la Secretaria de Educación Pública and from Fondo de Ayuda a la Investigación, Universidad Autónoma de San Luis Potosí, Mexico, under Grant No. C87-FAI-10.

[1]M. C. Cadeville and J. L. Morán-López, Phys. Rep. **153**, 331 (1987).

[2]C. E. Dahmani, M. C. Cadeville, J. M. Sanchez, and J. L. Morán-López, Phys. Rev. Lett. **55**, 1208 (1985).

[3]G. Inden, in *Alloy Phase Diagrams,* edited by L. H. Bennett, T. B. Massalski, and B. C. Giessen (North-Holland, New York, 1983), p. 175.

[4]F. J. Martinez-Herrera, F. Mejia-Lira, F. Aguilera-Granja, and J. L. Morán-López, Phys. Rev. B **31**, 1686 (1985).

[5]R. Hawkins and J. M. Sanchez, J. Phys. F **18**, 767 (1988).

[6]C. R. Houska, J. Phys. Chem. Solids **24**, 95 (1963); D. A. Lavis and W. M. Fairbairn, Philos. Mag. **13**, 477 (1966); H. Sagane and K. Oki, Trans. Jpn. Inst. Met. **21**, 811 (1980).
[7]P. R. Swann, W. R. Duff, and R. M. Fisher, Metall. Trans. **3**, 409 (1972).
[8]W. Koster and T. Godecke, Z. Metallkd. **71**, 765 (1980).
[9]J. Büth and G. Inden, Acta Metall. **30**, 213 (1982).
[10]G. Inden and W. Pitsch, Z. Metallkd. **63**, 253 (1972).
[11]B. Dünweg and K. Binder, Phys. Rev. B **36**, 6935 (1987).
[12]J. M. Sanchez and C. H. Lin, Phys. Rev. B **30**, 1448 (1984).
[13]J. Kanamori, Prog. Theor. Phys. **35**, 16 (1966).
[14]S. M. Allen and J. W. Cahn, Acta Metall. **20**, 423 (1972).
[15]J. M. Sanchez and D. de Fontaine, in *Structure and Bonding in Crystals,* edited by M. O'Keeffe and A. Navrotsky (Academic, New York, 1981), Vol. II, p. 117.
[16]A. Finel and F. Ducastelle, in *Phase Transformations in Solids,* edited by T. Tsakalakos (North-Holland, Amsterdam, 1984), p. 293.
[17]R. Kikuch, Phys. Rev. **81**, 988 (1951); J. Chem. Phys. **66**, 3352 (1977).
[18]J. M. Sanchez, D. Gratias, and F. Ducastelle, Physica A **128**, 334 (1984).